

RESEARCH

Open Access



# Receptor activity-modifying protein 1 regulates mouse skin fibroblast proliferation via the Gai3-PKA-CREB-YAP axis

Siyuan Yin<sup>1,2,3</sup>, Ru Song<sup>1,2</sup>, Jiayu Ma<sup>1,2</sup>, Chunyan Liu<sup>2,3</sup>, Zhenjie Wu<sup>1,2</sup>, Guoqi Cao<sup>1,2</sup>, Jian Liu<sup>2,3</sup>, Guang Zhang<sup>1,2</sup>, Huayu Zhang<sup>1,2</sup>, Rui Sun<sup>1,2</sup>, Aoyu Chen<sup>2,3</sup> and Yibing Wang<sup>1,2,3\*</sup> 

## Abstract

**Background:** Skin innervation is crucial for normal wound healing. However, the relationship between nerve receptors and wound healing and the intrinsic mechanism remains to be further identified. In this study, we investigated the role of a calcitonin gene-related peptide (CGRP) receptor component, receptor activity-modifying protein 1 (RAMP1), in mouse skin fibroblast (MSF) proliferation.

**Methods:** In vivo, Western blotting and immunohistochemical (IHC) staining of mouse skin wounds tissue was used to detect changes in RAMP1 expression. In vitro, RAMP1 was overexpressed in MSF cell lines by infection with Tet-On-Flag-RAMP1 lentivirus and doxycycline (DOX) induction. An InCuCyte S3 Live-Cell Analysis System was used to assess and compare the proliferation rate differences between different treatment groups. Total protein and subcellular extraction Western blot analysis, quantitative real-time-polymerase chain reaction (qPCR) analysis, and immunofluorescence (IF) staining analysis were conducted to detect signalling molecule expression and/or distribution. The CUT & RUN assay and dual-luciferase reporter assay were applied to measure protein-DNA interactions.

**Results:** RAMP1 expression levels were altered during skin wound healing in mice. RAMP1 overexpression promoted MSF proliferation. Mechanistically, total Yes-associated protein (YAP) and nuclear YAP protein expression was increased in RAMP1-overexpressing MSFs. RAMP1 overexpression increased inhibitory guanine nucleotide-binding protein (G protein)  $\alpha$  subunit 3 (Gai3) expression and activated downstream protein kinase A (PKA), and both elevated the expression of cyclic adenosine monophosphate (cAMP) response element-binding protein (CREB) and activated it, promoting the transcription of *YAP*, elevating the total YAP level and promoting MSF proliferation.

**Conclusions:** Based on these data, we report, for the first time, that changes in the total RAMP1 levels during wound healing and RAMP1 overexpression alone can promote MSF proliferation via the Gai3-PKA-CREB-YAP axis, a finding critical for understanding RAMP1 function, suggesting that this pathway is an attractive and accurate nerve target for skin wound treatment.

**Keywords:** RAMP1, Fibroblast proliferation, PKA, CREB, YAP, Transcription factor, Wound healing

## Background

Based on its surface area, the skin is the largest organ in humans [1–3], and skin wound healing is a dynamic and highly regulated and coordinated process involving haemostasis, inflammation, angiogenesis, growth, re-epithelialization and remodelling [4]. In this process, fibroblasts

\*Correspondence: ybwang@sdfmu.edu.cn

<sup>3</sup> Department of Plastic Surgery, The First Affiliated Hospital of Shandong First Medical University & Shandong Provincial Qianfoshan Hospital, Jinan 250014, Shandong, People's Republic of China  
Full list of author information is available at the end of the article



play a crucial role from the late inflammatory phase to final epithelization through secretion, migration, proliferation and transdifferentiation [3, 5].

Nerves and neuromodulators, including calcitonin gene-related peptide (CGRP), play essential roles in different steps of the skin wound healing process [6, 7] by targeting all skin tissues and cells, including keratinocytes, fibroblasts, vascular endothelial cells and immune cells [7–11]. Damaged or abnormal nerves and/or nerve function can result in chronic wounds [12]; additionally, neurogenic stimuli can promote the repair not only of denervation-related wounds but also of ulcers, ischaemic wounds and other chronic wounds [13–15], among which CGRP, a 37-amino acid neuropeptide, is an attractive candidate [16]. However, the short half-life of CGRP in plasma limits its long-term application [17]; therefore, we focused on its receptor, which is a heterodimer comprising three subunits: a seven-transmembrane guanine nucleotide-binding protein (G protein)-calcitonin receptor-like receptor (CLR), receptor activity-modifying protein 1 (RAMP1) and receptor component protein (RCP) [16, 18]. RAMP1 is a small protein with a single transmembrane domain that, in addition to endowing CGRP with binding specificity, regulates receptor trafficking, signalling and cell proliferation, migration and differentiation [19]. RAMP1 is highly expressed in skin cells and is related to wound healing. Chie et al. [20] reported that RAMP1 plays a critical role in wound healing by promoting angiogenesis and lymphangiogenesis. Additionally, Toshiaki et al. [21] reported that RAMP1 can stimulate lymphangiogenesis and restore lymphatic flow to improve lymphedema. However, no direct study on RAMP1 and skin fibroblasts has been performed.

Yes-associated protein (YAP) is a downstream effector of the Hippo pathway and plays an essential role in the control of cell proliferation and survival. YAP is also important for wound healing and is highly expressed in fibroblasts inside and outside the wound bed in the early wound healing phase [22–24]. G protein-coupled receptor (GPCR)-mediated signalling can modulate YAP/TAZ activity either positively or negatively, depending on the different cell types and various signals, receptors, and adaptor proteins involved [25]. As a class-B family [26] GPCR protein, CGRP, in conjunction with RAMP1, can stimulate YAP/TAZ expression and activity to promote liver regeneration [27]. The classical pathway of GPCRs involves stimulatory  $G\alpha$  subunit ( $G\alpha_s$ ) proteins stimulating adenylyl cyclase (AC) to produce cyclic adenosine monophosphate (cAMP) and elicit protein kinase A (PKA) and downstream cAMP response element-binding protein (CREB), while the inhibitory  $G\alpha$  subunit ( $G\alpha_i$ ) protein inhibits this process [28]. However, the  $G_i$  protein can stimulate AC2 to activate PKA and its downstream

signalling cascade [29]. Yu et al. [30] reported that PKA can phosphorylate YAP and modulate cell proliferation and differentiation. Similarly, using inducible PKA transgenic mice, Zhang et al. [31] found that CLR can activate PKA and prevent YAP activation and nuclear translocation. Wang [32] discovered that CREB interacts with YAP to promote liver cancer tumorigenesis. Considering these previous studies, we aimed to demonstrate the function of RAMP1 in skin fibroblasts, determine whether YAP is the main effector of RAMP1, and then identify the downstream pathway.

In the current study, we proved that RAMP1 expression levels are altered during skin wound healing in mice, constructed a RAMP1-overexpressing mouse skin fibroblast (MSF) cell line and found that RAMP1 promoted the proliferation of these MSFs through the  $G\alpha_i$ -PKA-CREB-YAP axis. This study provides new insights into the effects of RAMP1 on fibroblasts and some hints to more accurately regulate nerve innervation during wound healing.

## Methods and materials

### Cell culture and reagents

The MSF cell line (Guangzhou Jennio Biotech Co., Ltd., Guangzhou, China) was grown in high glucose (4.5 g/L glucose) Dulbecco's modified Eagle's medium (DMEM; Gibco, Thermo Fisher Scientific, MA, USA) with 10% tetracycline-free foetal bovine serum (FBS; Gibco) and maintained at 37 °C in a humidified 5% CO<sub>2</sub> incubator. The cells were treated with H-89 dihydrochloride (1 μM; CAS. 130964-39-5; MedChemExpress, LLC, USA), bucladesine sodium (BUC; 0.01 μM; CAS. 16980-89-5; MedChemExpress), verteporfin (VP; 0.01 μM; CAS. 129497-78-5; MedChemExpress), KG-501 (10 μM; CAS. 18228-17-6; MedChemExpress) or the relative concentration of solvent dimethyl sulfoxide (DMSO; CAS. 67-68-5; MP Biomedicals, LLC, USA).

### Doxycycline (DOX)-inducible lentivirus infection and small interfering RNA transfection

MSFs were infected with Tet-On-Flag-RAMP1 lentivirus or Tet-On-Flag-vector lentivirus (GeneChem Co., Ltd., Shanghai, China) for 24 h (the primer sequences used are shown in Additional file 1: Table S1), and then the cells were selected with growth medium containing puromycin (3 μg/ml; CAS. 58-58-2; Beijing Solarbio Science & Technology Co., Ltd., Beijing, China) for 48 h to obtain stable and highly pure clones. These clones were then treated with DOX (5 μg/ml; CAS. 564-25-0; MedChemExpress) to induce the expression of Flag-RAMP1 or its control form. RAMP1 overexpression MSFs were reverse-transfected with 50 nM small interfering RNAs (siRNAs) specifically targeting  $G\alpha_i3$  (si $G\alpha_i3$ -1 and si $G\alpha_i3$ -2; Guangzhou RiboBio Co., Ltd., Guangzhou,

China) or a negative control sequence (siNC; RiboBio) using RiboBio transfection reagent. After 48 h, the cells were harvested for RNA and protein extraction and detection. The gene sequences used for the Gai3 siRNA and its negative control are provided in Additional file 1: Table S2.

#### Cell proliferation assay

MSFs with different treatments were seeded in a 96-well plate (Corning Incorporated, USA) at an initial 3000 cells per well, and then the plate was placed in an IncuCyte S3 Live-Cell Analysis System, where real-time images were captured every 6 h for 72 h or 2000 cells per well were imaged for 96 h. Photographs of the cells were taken from two separate regions of each well using a 10× objective. Values from the two regions of each well were pooled and averaged across three replicates, and the proliferation rate was determined as the area confluence ratio normalized to hour 0 using IncuCyte S3 software (Essen BioScience, Ann Arbor, MI, USA).

#### Animals

C57BL/6J male mice (8–10 weeks old; weight 30–35 g) (Beijing Vital River Laboratory Animal Technology Co., Ltd, Beijing, China) were used as a skin wound model in this study. All the animals were housed individually under a 12:12 h light/dark cycle at a controlled constant temperature ( $25 \pm 1$  °C) and humidity ( $60 \pm 5\%$ ). All the experiments were approved by the ethics committee of The First Affiliated Hospital of Shandong First Medical University & Shandong Provincial Qianfoshan Hospital (Approval Number: SYDWLS[2021]002) and were performed in accordance with the guidelines and regulations.

#### Skin wound model and evaluation of wound healing

After anaesthesia with 1% pentobarbital sodium, the mouse was depilated and disinfected. On both side of the dorsal part, approximately 7 mm away from midline, 2 points 4 cm away from the base of the neck were marked as the central points of the wound preparation. Next, a sterile, disposable 5 mm biopsy punch tool was used to create a circular wound outline at this point, along with a pair of iris scissors (with curved tips) to excise the circular piece of tissue to make a full-thickness wound. The time of wound induction was defined as hour 0. After wound preparation was completed, the mice were housed individually (one mouse per cage).

Twenty male mice were randomly divided into five groups: (1) siGai3-2 group (treated with 5 nmol); (2) VP group (treated with 100 nmol VP); (3) H-89 group (treated with 100 nmol H-89); (4) BUC group (treated with 100 nmol BUC); and (5) KG-501 group (treated

with 100 nmol KG-501). 24 h (days 1) after wound induction, the diluent was subcutaneously administered at the edge of the wound of the right side for 7 consecutive days, while the wound of the left side was administered siNC (5 nmol) or DMSO at a coordinated dose (10  $\mu$ l) as a self-control. At hours 0 (days 0), 24 h (days 1) and days 3, 5 and 7 postinjury, a ruler was placed below the wound, and the wound was photographed at a fixed height for wound healing evaluation. The wound healing rate was calculated as a percentage of the initial wound area by defining the initial wound area as 0% closure using ImageJ software (U.S. National Institutes of Health, Bethesda, MD, USA).

#### Skin wound tissue sample process

A total of 12 male C57BL/6J mice (8–10 weeks old; weight 30–35 g) were used for skin wound tissue sample process. At 24 h (days 1) and days 3, 5 and 7 after wound excision, three randomly selected mice were anaesthetized, and the periwound skin was lifted with forceps. The wound tissue, including an additional 3 mm of normal skin around the wound, was harvested with a scalpel and divided into two parts along with the central axis.

Half of the above tissue was divided into two parts and rapidly frozen in a 1.5 ml snap cap tube in liquid nitrogen and stored at  $-80$  °C for subsequent molecular analysis. Wound tissue protein was extracted using a Minute™ Total Protein Extraction Kit for Skin Tissue (#SA-01-SK, Invent Biotechnologies, Inc., USA).

The other half of the above tissue was fixed in 10% formalin solution, embedded in paraffin and sectioned at 3  $\mu$ m for histochemical analyses which were performed by haematoxylin–eosin (H&E) staining and immunohistochemical (IHC) staining. Deparaffinization, rehydration, antigen retrieval, endogenous peroxidase blocking, and goat serum (#SP-9001; ZSGB-BIO, Beijing, China) blocking of paraffin sections were performed as previously described [33–35]. Next, the wound skin tissue sections were incubated with primary antibody against RAMP1 (#ab156575; Abcam Plc, Cambridge, UK) at a dilution of 1:200 at 4 °C overnight. On the second day, all sections were incubated with biotin-labelled goat anti-rabbit IgG polymer for 15 min at room temperature and incubated with horseradish enzyme-labelled streptavidin working solution for 15 min at room temperature. Finally, the slides were counterstained with diaminobenzidine (DAB; #ZLI-9018, ZSGB-BIO) and haematoxylin (CAS. 517-28-2; Beijing Solarbio Science & Technology). For H&E staining, after deparaffinization and rehydration, slides were stained with haematoxylin and eosin (CAS. 17372-87-1; Beijing Solarbio Science & Technology) according to the manufacturer's instructions. All the sections were then dehydrated, cleared, and sealed. The

images were observed and captured using an Olympus IX73 microscope (Olympus, Tokyo, Japan). The mean density was calculated as the integrated optical density (IOD)/area using ImageJ software.

#### Subcellular fractionation

To separate cytosolic and nuclear fractions, a Minute™ cytoplasmic and nuclear extraction kit (#SC-003; Invent Biotechnologies) was used according to the manufacturer's protocol. Briefly, cells were washed in cold phosphate-buffered saline (PBS; #B310KJ, Shanghai BasalMedia Technologies Co., Ltd., Shanghai, China) and lysed following incubation with cytoplasmic extraction buffer on ice for 5 min with vigorous vortexing for 15 s. Next, the lysates were centrifuged at 14,000 g for 5 min at 4 °C to obtain the cytosolic and membrane fractions (supernatant) and nuclear fraction (pellet). The nuclear pellet was then washed with PBS three times, lysed with nuclear extraction buffer while undergoing vigorous vortexing and centrifuged in a prechilled filter cartridge with a collection tube to obtain the nuclear extract.

#### Western blot analysis

Western blot analysis was performed as previously described [36]. The following antibodies and reagents used: primary antibodies against Flag (#14793), PCNA (#13110), PKA C- $\alpha$  (#4782), CREB (#9197), pCREB (S133) (#9198), YAP (#14074) and pYAP (S127) (#13008) were purchased from Cell Signaling Technology, Inc. (diluted 1:1000; CST, MA, USA), a primary antibody against RAMP1 (#ab156575) was purchased from Abcam Plc (diluted 1:1000; Cambridge, UK), and a primary antibody against Gai3 (#sc-365422) was purchased from Santa Cruz Biotechnology, Inc. (diluted 1:500; TX, USA); horseradish peroxidase (HRP)-linked anti-rabbit IgG (#7074) and HRP-linked anti-mouse IgG (#7076) secondary antibodies were purchased from CST (diluted 1:5000); and total protein-labelling No-Stain™ reagent (#A44449) was purchased from Thermo Fisher Scientific.

#### Quantitative real-time polymerase chain reaction (qPCR) analysis

RNA isolation and reverse transcription were performed according to our previously reported method [36]. Quantitative analysis was performed using a SYBR® Green Premix *Pro Taq* HS qPCR kit (#AG11701; Accurate Biotechnology, Hunan, China) and the QuantStudio™ 3 real-time PCR system (Applied Biosystems, Thermo Fisher Scientific) according to the manufacturer's instructions.  $\beta$ -Actin mRNA was used as an internal control, and the primers used are shown in Additional file 1: Table S3.

#### Immunofluorescence (IF) staining

MSFs subjected to different treatments were washed with PBS, fixed with 4% paraformaldehyde (#P0099; Beyotime Institute of Biotechnology, Jiangsu, China) at room temperature for 10 min and permeabilized with immunostaining permeabilization buffer (#P0097; Beyotime) for 10 min. Next, slides with cells were incubated with primary antibody at 4 °C overnight and then with secondary antibody anti-rat Alexa Fluor-488 (#4416; diluted 1:200; CST), anti-rat Alexa Fluor-555 (#4417; diluted 1:200; CST), anti-rabbit Alexa Fluor-488 (#4412; diluted 1:200; CST) or anti-rabbit Alexa Fluor-555 (#4413; diluted 1:200; CST) at room temperature for 1 h. Nuclei were stained with DAPI (#62248; Thermo Fisher Scientific) at room temperature for 30 min. Finally, the slides were covered with ProLong Gold antifade reagent (#P36934; Invitrogen), observed and recorded using a Nikon Eclipse Ti2 confocal microscope (Nikon Instruments (Shanghai) Co., Ltd., Shanghai, China). The following primary antibodies were used: rabbit anti-Flag (#14793), anti-PCNA (#13110), anti-YAP (#14074), and anti-CREB (#9197), all diluted 1:200 and purchased from CST, and rat anti-Actin (#ab130935) was diluted 1:200 and purchased from Abcam.

#### CUT & RUN assay

Protein-DNA interactions were analysed using cleavage under targets and release using a nuclease (CUT&RUN) assay kit (#86652; CST) following the manufacturer's instructions. Approximately 100,000 cells were used for each reaction at room temperature. The positive control was a rabbit monoclonal antibody (mAb) against trimethylated histone H3 (Lys4) (H3K4me3; #9751), and the negative control was a rabbit mAb IgG isotype (#66362), which was provided in the kit. They were used with an anti-CREB antibody (diluted 1:50; #9197; CST) for binding and the subsequent cleavage and release steps. The extracted DNA was purified using DNA purification buffers and spin columns (#14209; CST). Finally, the DNA products were quantified by qPCR and DNA agarose gel electrophoresis, and the primers used are shown in Additional file 1: Table S3.

#### Dual-luciferase reporter assay

The CREB control plasmid, CREB plasmid, firefly luciferase plasmid with the YAP-CREB-binding site (CBS) wild-type promoter, firefly luciferase plasmid with the YAP-CBS mutation promoter and Renilla luciferase plasmid were all purchased from Syngentech (Beijing Syngentech Co., Ltd., Beijing, China) and used to transfect HEK293T cells (#CTCC-001-0188; Meisen Chinese Tissue Culture Collections, Zhejiang, China). Next, the luciferase activity was analysed using a dual-luciferase

reporter kit (# RG027; Beyotime) and an iMark Microplate Absorbance Reader (Bio-Rad Laboratories, Inc., CA, USA). The firefly luciferase data were normalized to the Renilla luciferase data and expressed as the fold change relative to the control. The dual-luciferase reporter assays were conducted for six replicates per group and repeated independently three times.

### Statistical analysis

The data for all experiments were shown as means  $\pm$  standard deviation (SD) of three biological replicates, and all data analyses were performed using GraphPad Prism 7 software (San Diego, CA). Statistical analysis between groups was performed using Student's *t* test to determine significance. *P* values  $< 0.05$  were considered statistically significant.

## Results

### RAMP1 overexpression promotes MSF proliferation

To investigate the changes in RAMP1 expression during skin wound healing, we first performed mouse skin wound tissue protein analysis using Western blotting and IHC staining (Fig. 1A–D). The RAMP1 content and mean optical density of RAMP1 in the dermis gradually increased from 24 h (days 1) to days 3 and days 5 post-injury. By days 7, when the wound area was healed by approximately 95%, the RAMP1 content decreased compared with that on days 5 but was still higher than that at 24 h (days 1). The dermis thickness measurements by H&E staining of the skin sections also showed the same trend (Fig. 1C, E). Given that fibroblasts are one of the most important cells of the dermis and in the wound healing process, we next explored the role of RAMP1 in MSF function. First, we infected MSFs with Tet-On-Flag-RAMP1 lentivirus and Tet-On-Flag-vector lentivirus. After DOX (5  $\mu$ g/ml) induction for 48 h, IF showed Flag expression in both the vector control (VEC) and RAMP1 overexpression (OE) group, and the fluorescence of the OE group was more intense (Fig. 1F). Additionally,

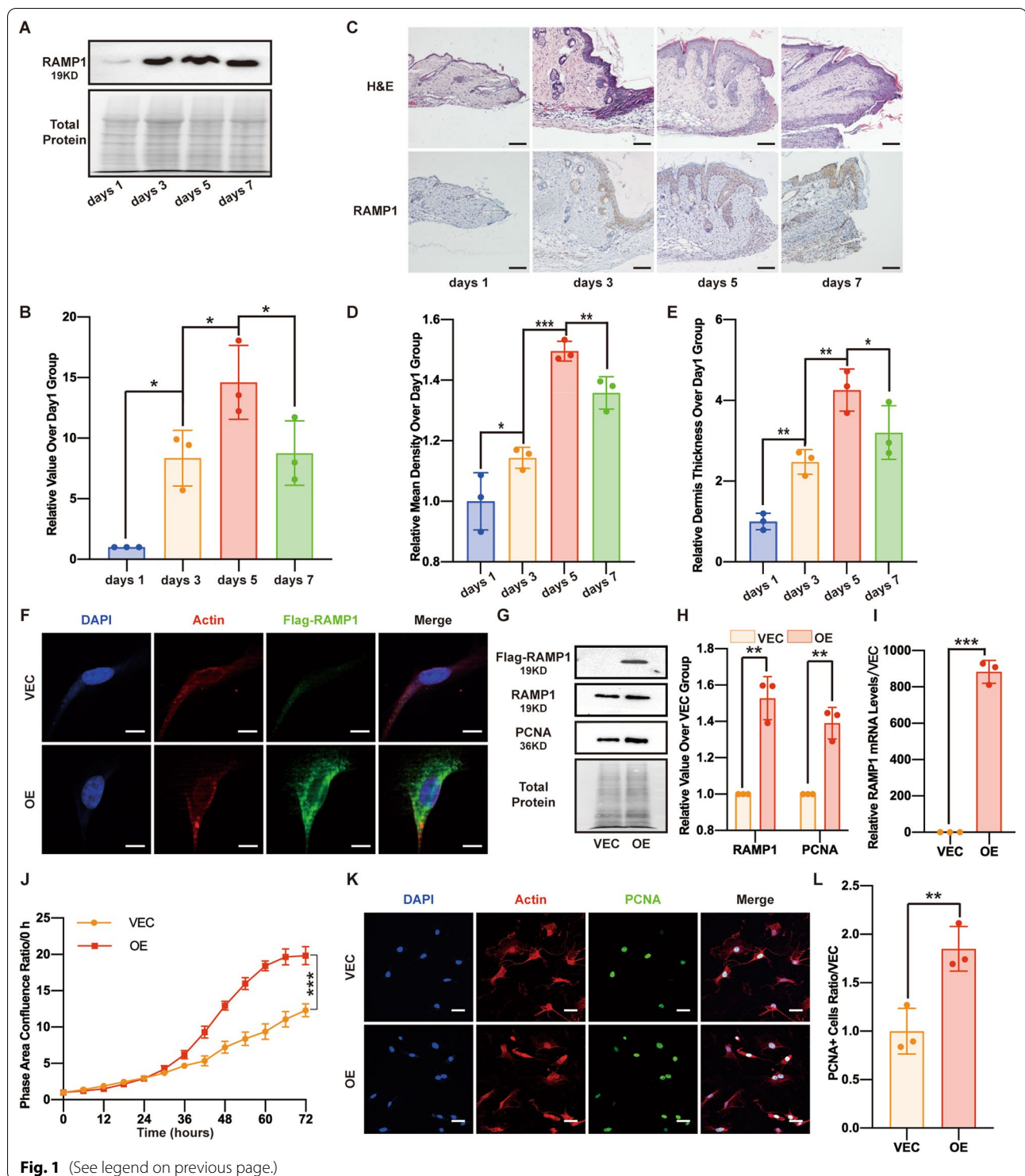
Western blot and qPCR analyses were performed to assess infection success, revealing that RAMP1 protein expression and mRNA transcription in the OE group were significantly higher than those in the VEC group (Fig. 1G–I). After successfully infecting RAMP1-overexpressing MSFs and vector MSFs, we conducted an MSF proliferation assay using an IncuCyte S3 system. The rate at which the MSFs reached confluence in an area was much faster in the OE group than in the VEC group (Fig. 1J). To confirm the reliability of the S3 results based on cell confluence area measurement, we examined PCNA expression in both groups by performing Western blotting and IF staining. As expected, PCNA expression was higher in the OE group than in the VEC group (Fig. 1G, H, K, L), consistent with the S3 proliferation results, indicating that RAMP1 upregulation can promote the proliferation ability of MSFs.

### RAMP1 overexpression increases Gai3, PKA, CREB and YAP expression

Because RAMP1 is an upstream factor in the context of the entire proliferation pathway, we explored the pathway downstream of regulatory RAMP1 during MSF proliferation to determine whether YAP is part of this pathway. We first evaluated YAP and pYAP (S127) in the MSFs of the OE and VEC groups. The expression of both YAP and pYAP (S127) was elevated when RAMP1 was overexpressed (Fig. 2A, B). qPCR analysis indicated that the YAP transcription level was also elevated in the OE group (Fig. 2C). YAP expression was higher in both the cytoplasmic and nuclear extracts in the OE group than in the VEC group (Fig. 2D, E, G). Considering that RAMP1 can interact with and modulate the activities of GPCRs and that YAP can be regulated by signalling mediated by GPCRs, we next examined the G protein subunits and classical factors in the pathway downstream of GPCRs. The expression of Gai3, PKA, CREB and its active form, pCREB (S133), was upregulated in the OE group (Fig. 2A, B). Additionally, subcellular fractionation was assessed by Western blotting and IF staining, and CREB expression

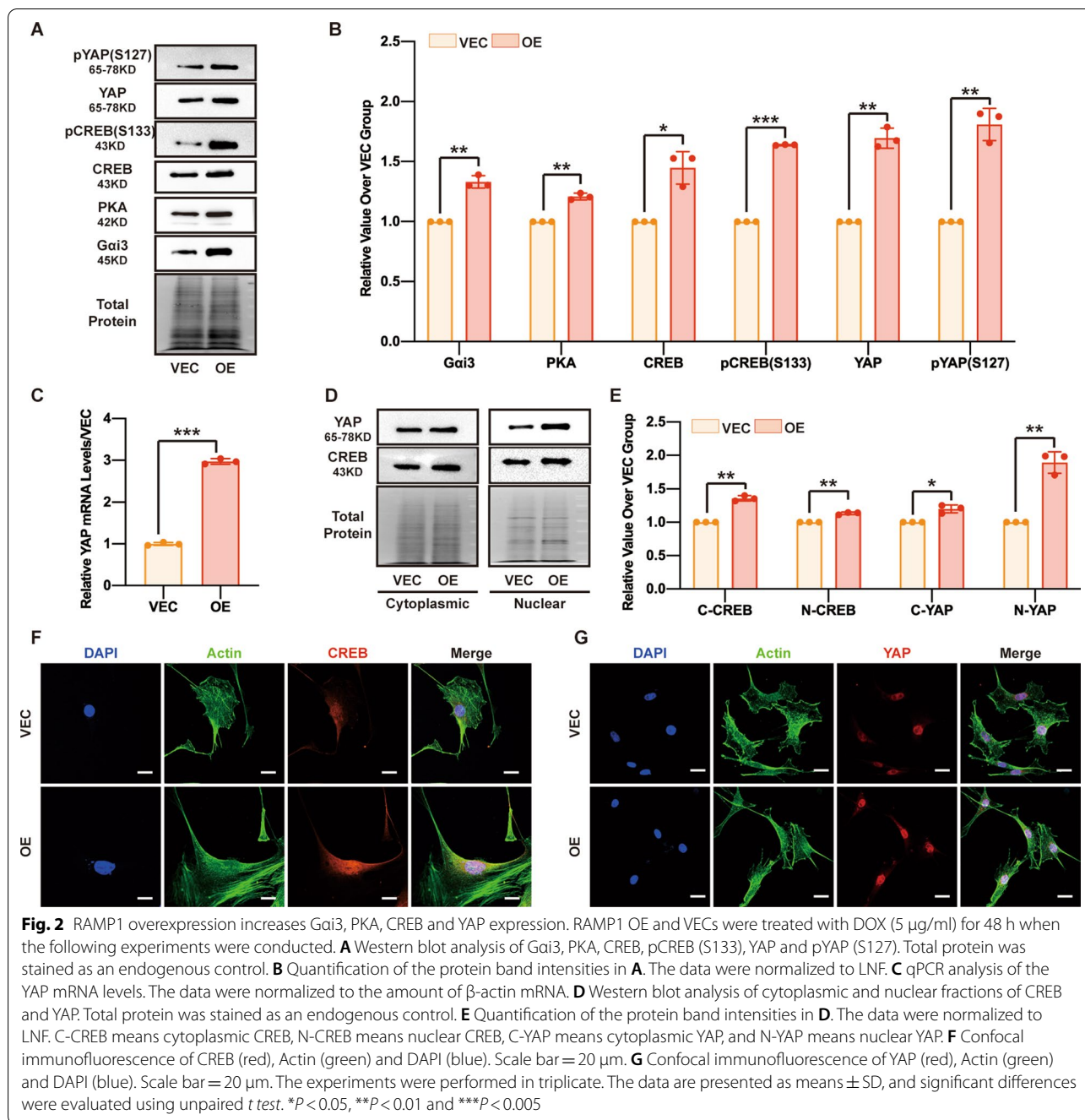
(See figure on next page.)

**Fig. 1** RAMP1 overexpression promotes cell proliferation. **A** Western blot analysis of RAMP1 in skin wound tissue proteins. Total protein was stained as an endogenous control. **B** Quantification of the protein band intensities in **A**. The data were normalized by lane normalization factor (LNF). **C** H&E staining and IHC staining of RAMP1 in skin wound tissue sections (10 $\times$ ). Scale bar = 100  $\mu$ m. **D** Quantitative analysis of RAMP1 expression by IHC staining of **C**. **E** Dermis thickness measurements by H&E staining of **C**. RAMP1 OE and VECs were treated with DOX (5  $\mu$ g/ml) for 48 h when the following experiments were conducted. **F** Confocal immunofluorescence of Flag (green), Actin (red) and DAPI (blue). Scale bar = 10  $\mu$ m. **G** Western blot analysis of Flag-RAMP1, RAMP1 and PCNA. Total protein was stained as an endogenous control. **H** Quantification of the protein band intensities of **G**. The data were normalized by LNF. **I** qPCR analysis of RAMP1 mRNA levels. The data were normalized to the amount of  $\beta$ -actin mRNA. **J** Cell proliferation ability (72 h) measured by confluence measurements normalized to hour 0 calculated using IncuCyte (Essen BioScience). **K** Confocal immunofluorescence of PCNA (green), Actin (red) and DAPI (blue). Scale bar = 20  $\mu$ m. **L** Dot plots show quantification of the frequency of PCNA-positive cells in each field of view. The experiments were performed in triplicate. The data are presented as means  $\pm$  SD, and significant differences were evaluated using unpaired *t* test. \**P* < 0.05, \*\**P* < 0.01 and \*\*\**P* < 0.005



was elevated in both the cytoplasm and nucleus (Fig. 2D–F). These data demonstrated that RAMP1 OE led to an increase in Gai3, PKA, CREB, pCREB (S133), YAP and

pYAP (S127) expression and that this effect may involve an axis downstream of regulatory RAMP1 during MSF proliferation.



**RAMP1 overexpression promotes proliferation by increasing YAP protein levels**

To elucidate whether the elevated expression and activity of YAP promoted MSF proliferation, verteporfin (VP, 0.01  $\mu$ M), a YAP inhibitor, was added during the culture of the MSF OE group (OE + VP group). After VP treatment, the MSF proliferation rate of the OE + VP group was significantly decreased compared with that of the RAMP1 OE group (Fig. 3A). Western blotting and IF

detection of PCNA also confirmed that the PCNA level was reduced in the OE + VP group (Fig. 3B, C, E, F). VP treatment also decreased the total YAP protein level in the OE + VP group (Fig. 3B, C). Cytoplasmic and nuclear extraction Western blotting and IF showed that cytoplasmic YAP and nuclear YAP levels were also decreased in the OE + VP group (Fig. 3G–I); however, qPCR analysis showed that VP treatment could not influence YAP transcription (Fig. 3D). Thus, VP directly prevented the

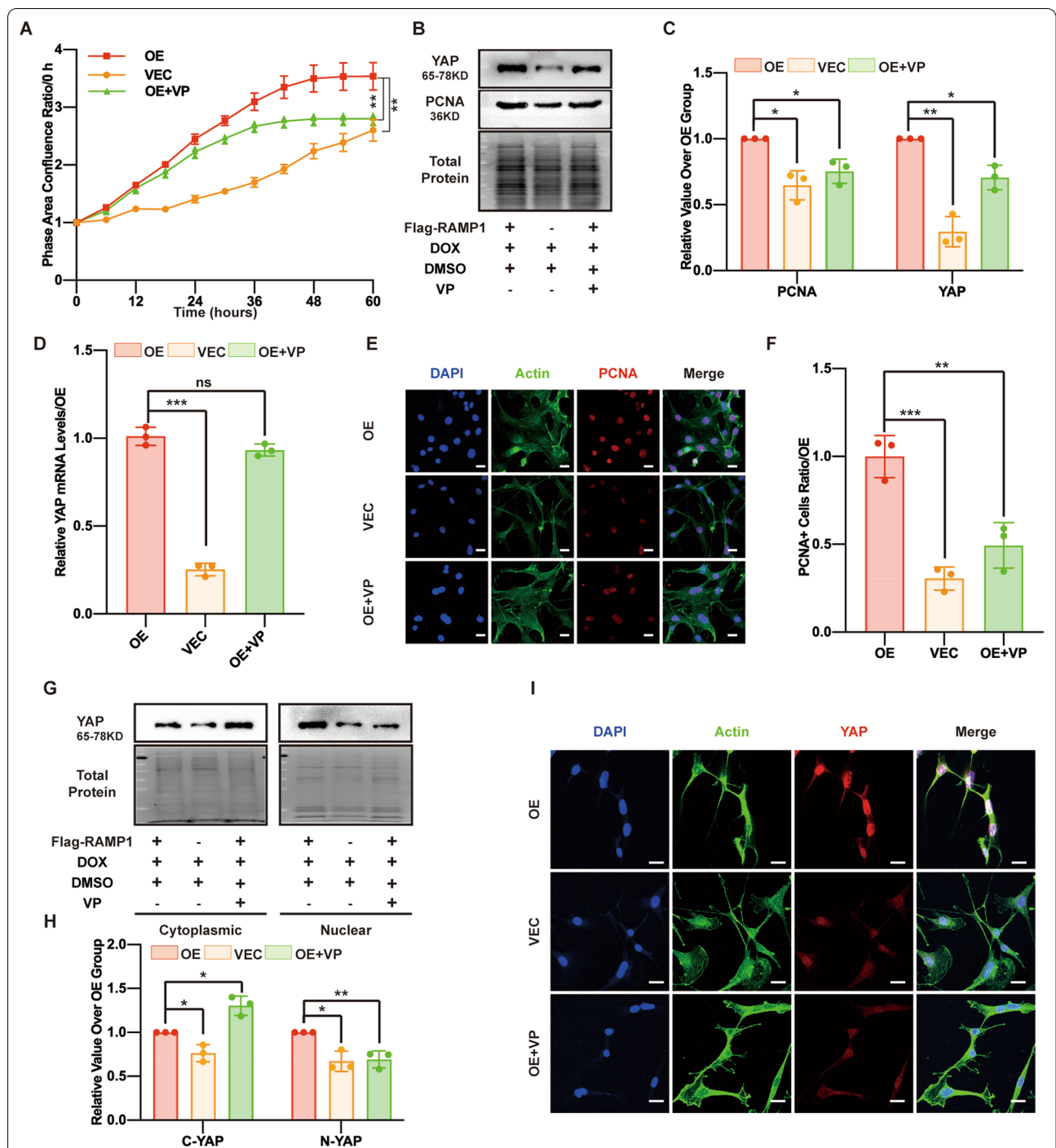


**Fig. 3** RAMP1 overexpression promotes proliferation by increasing YAP protein levels. In the OE+VP group, RAMP1 OE cells were first treated with veterporfin (VP, 0.01  $\mu$ M) alone for 12 h and then with VP (0.01  $\mu$ M) and DOX (5  $\mu$ g/ml) for 48 h. In the OE and VEC groups, RAMP1 OE and VECs were first treated with DMSO (0.01  $\mu$ M) alone for 12 h and then with DMSO (0.01  $\mu$ M) and DOX (5  $\mu$ g/ml) for 48 h. **A** Cell proliferation ability measured by confluence measurements normalized to hour 0 and calculated using IncuCyte (Essen BioScience). **B** Western blot analysis of PCNA and YAP. Total protein was stained as an endogenous control. **C** Quantification of the protein band intensities in **B**. The data were normalized to PCNA and YAP. **D** qPCR analysis of the YAP mRNA levels. The data were normalized to the amount of  $\beta$ -actin mRNA. **E** Confocal immunofluorescence of PCNA (red), Actin (green) and DAPI (blue). Scale bar = 20  $\mu$ m. **F** The dot plots show quantification of the frequency of PCNA-positive cells in each field of view. **G** Western blot analysis of the cytoplasmic and nuclear fractions of YAP. Total protein was stained as an endogenous control. **H** Quantification of the protein band intensities of **G**. The data were normalized to LNF. C-YAP means cytoplasmic YAP, and N-YAP means nuclear YAP. **I** Confocal immunofluorescence of YAP (red), Actin (green) and DAPI (blue). Scale bar = 20  $\mu$ m. All the experiments were performed in triplicate. The data are presented as means  $\pm$  SD, and significant differences were evaluated using unpaired *t* test. \**P* < 0.05, \*\**P* < 0.01 and \*\*\**P* < 0.005

YAP-TEAD interaction and its downstream signalling, leading to YAP sequestration in the cytoplasm and degradation, but did not directly prevent YAP protein expression [37]. In addition to the in vitro findings, the in vivo application of VP (100 nmol) to mouse wounds delayed wound healing (Additional file 2: Fig. S1A and S1B), indicating that YAP inhibition could ameliorate wound healing. The data confirmed that YAP is the downstream effector of RAMP1 regulation of MSF proliferation.

#### Interference with *Gai3* after RAMP1 overexpression decreases PKA, CREB and YAP expression and MSF proliferation

To identify the mechanism by which RAMP1 regulates YAP expression, *Gai3* siRNA was first used to silence *Gai3* activity of RAMP1 OE cells in the si*Gai3*-1 and si*Gai3*-2 groups, while a negative control sequence was used in the siNC group as a control (Fig. 4A–C). *Gai3* interference decreased the proliferation rate of MSFs (Fig. 4D), and the Western blot and IF staining analyses of PCNA expression also demonstrated the inhibitory effect of *Gai3* interference on MSF proliferation (Fig. 4F–I). Next, we detected the downstream protein levels, revealing that PKA, CREB and YAP levels were downregulated after *Gai3* interference and the YAP transcription level was also decreased (Fig. 4E–G). The level of pCREB (S133), which is the active form of CREB, was decreased in the si*Gai3*-1 group and si*Gai3*-2 group. Additionally, the level of pYAP (S127), which is the inactive form of YAP, was decreased in both *Gai3* interference groups (Fig. 4F, G). Because both YAP and CREB function in the nucleus, we performed Western blotting and IF staining on the extracted cytoplasmic and nuclear fractions to identify the nuclear protein level. Both YAP and CREB levels in the nucleus were significantly lower in the si*Gai3*-1 and si*Gai3*-2 groups than in the siNC group, and *Gai3* silencing led to reduced cytoplasmic localization of YAP and CREB (Fig. 4J–M). The nonhealing rate

of wounds on the si*Gai3*-2 (5 nmol) side at 24 h (days 1), days 3, days 5 and days 7 was significantly higher than that of wounds on the siNC side at the corresponding time points (Additional file 2: Fig. S1C and S1D), indicating that inhibition of *Gai3* delayed the healing of mouse wounds. These results suggest that RAMP1 may regulate YAP by modulating *Gai3* expression.

#### The PKA inhibitor H-89 reduces CREB and YAP levels and inhibits MSF proliferation

Many signalling molecules might participate in the processes between RAMP1-*Gai3* axis activation and YAP activity regulation. Because PKA, CREB and pCREB (S133) were upregulated in the RAMP1 OE group and downregulated in the *Gai3* interference group, we asked whether PKA is a downstream factor of *Gai3* and an upstream factor of YAP. By treating the RAMP1 OE group with the PKA inhibitor H-89 dihydrochloride (H-89; 1  $\mu$ M; OE+H-89 group), we observed a diminished proliferation rate in the S3 cell proliferation analysis and consistently decreased PCNA expression by Western blotting (Fig. 5A, B, D). H-89 also reduced the PKA, CREB and YAP protein levels and YAP transcription levels, and pCREB (S133) and pYAP (S127) were downregulated in the OE + H-89 group (Fig. 5A–C). Additionally, we measured the YAP and CREB protein levels in both the cytoplasmic and nuclear extract fractions and by IF staining to determine the effect of H-89 on effector localization. H-89 reduced the YAP and CREB levels in the nucleus and cytoplasm (Fig. 5E–H). The optical images and statistical analysis showed that topical continuous treatment with H-89 decreased the wound healing rate compared with that of the DMSO control group, particularly in the early phase (Additional file 2: Fig. S1E and S1F), indicating that H-89 treatment may delay wound healing by inhibiting PKA. These results indicate that RAMP1-*Gai3* may regulate PKA function to modulate downstream effects.

(See figure on next page.)

**Fig. 4** Interference with *Gai3* after RAMP1 overexpression decreases PKA, CREB, and YAP expression and MSF proliferation. RAMP1 OE cells were reverse-transfected with 50 nM of small interfering RNAs (siRNAs) specifically targeting *Gai3* (si*Gai3*-1 and si*Gai3*-2) or a negative control sequence (siNC) for 48 h and then were treated with DOX (5  $\mu$ g/ml) for 48 h. **A** Western blot analysis of *Gai3*. Total protein was stained as an endogenous control. **B** Quantification of the protein band intensities of **A**. The data were normalized to LNF. **C** qPCR analysis of the *Gai3* mRNA levels. The data were normalized to the amount of  $\beta$ -actin mRNA. **D** Cell proliferation ability measured by confluence measurements normalized to hour 0 calculated using IncuCyte (Essen BioScience). **E** qPCR analysis of the YAP mRNA levels. The data were normalized to the amount of  $\beta$ -actin mRNA. **F** Western blot analysis of PCNA, PKA, CREB, pCREB (S133), YAP, and pYAP (S127). Total protein was stained as an endogenous control. **G** Quantification of the protein band intensities in **F**. The data were normalized to LNF. **H** Confocal immunofluorescence of PCNA (red), Actin (green) and DAPI (blue). Scale bar = 20  $\mu$ m. **I** Dot plots show quantification of the frequency of PCNA-positive cells in each field of view. **J** Western blot analysis of the cytoplasmic and nuclear fractions of CREB and YAP. Total protein was stained as an endogenous control. **K** Quantification of the protein band intensities of **J**. The data were normalized to LNF. C-CREB means cytoplasmic CREB, N-CREB means nuclear CREB, C-YAP means cytoplasmic YAP, and N-YAP means nuclear YAP. **L** Confocal immunofluorescence of CREB (red), Actin (green) and DAPI (blue). Scale bar = 20  $\mu$ m. **M** Confocal immunofluorescence of YAP (red), Actin (green) and DAPI (blue). Scale bar = 20  $\mu$ m. The experiments were performed in triplicate. The data are presented as means  $\pm$  SD, and significant differences were evaluated using unpaired *t* test. \* $P$  < 0.05, \*\* $P$  < 0.01, \*\*\* $P$  < 0.005 and ns, not significant

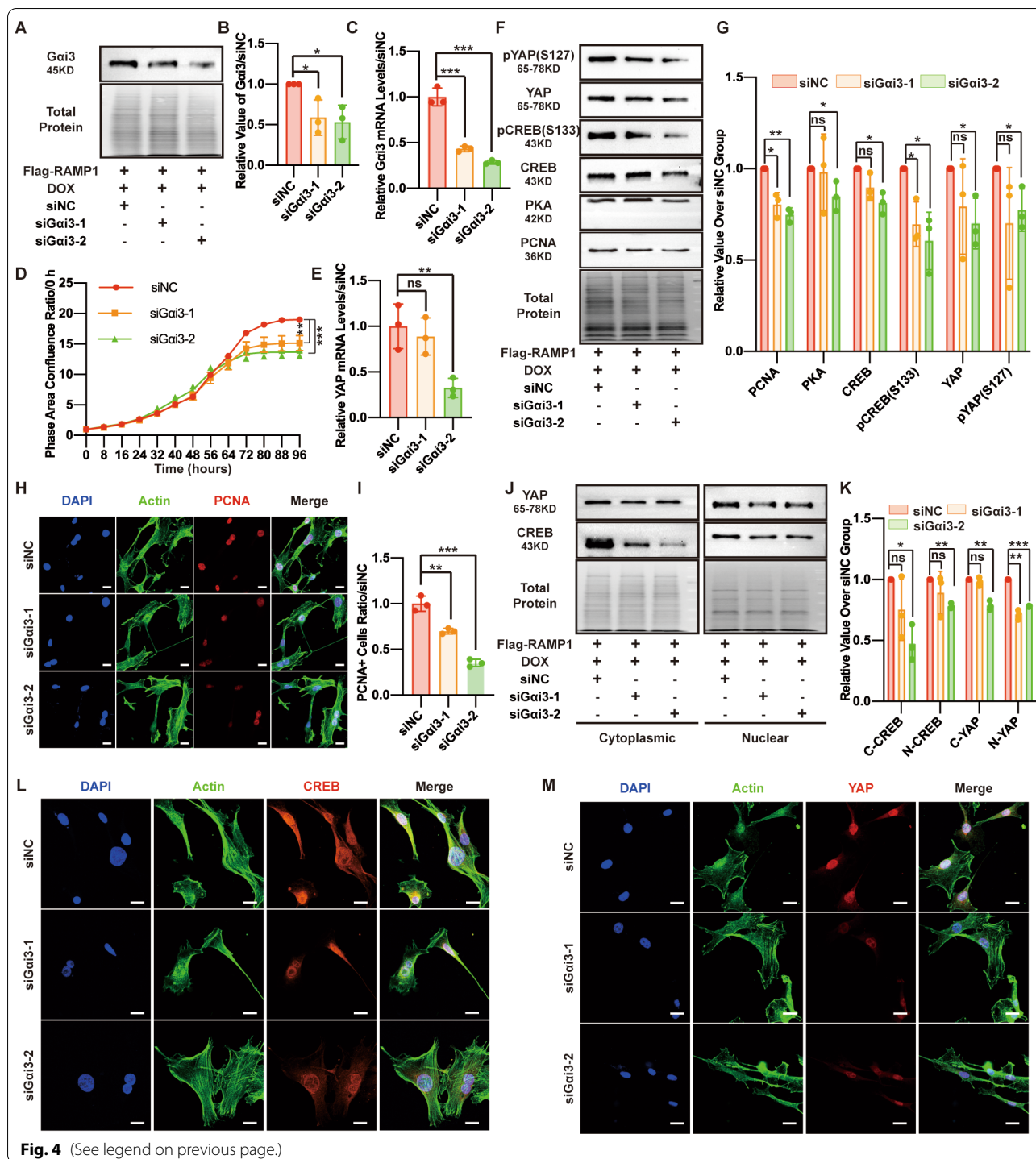
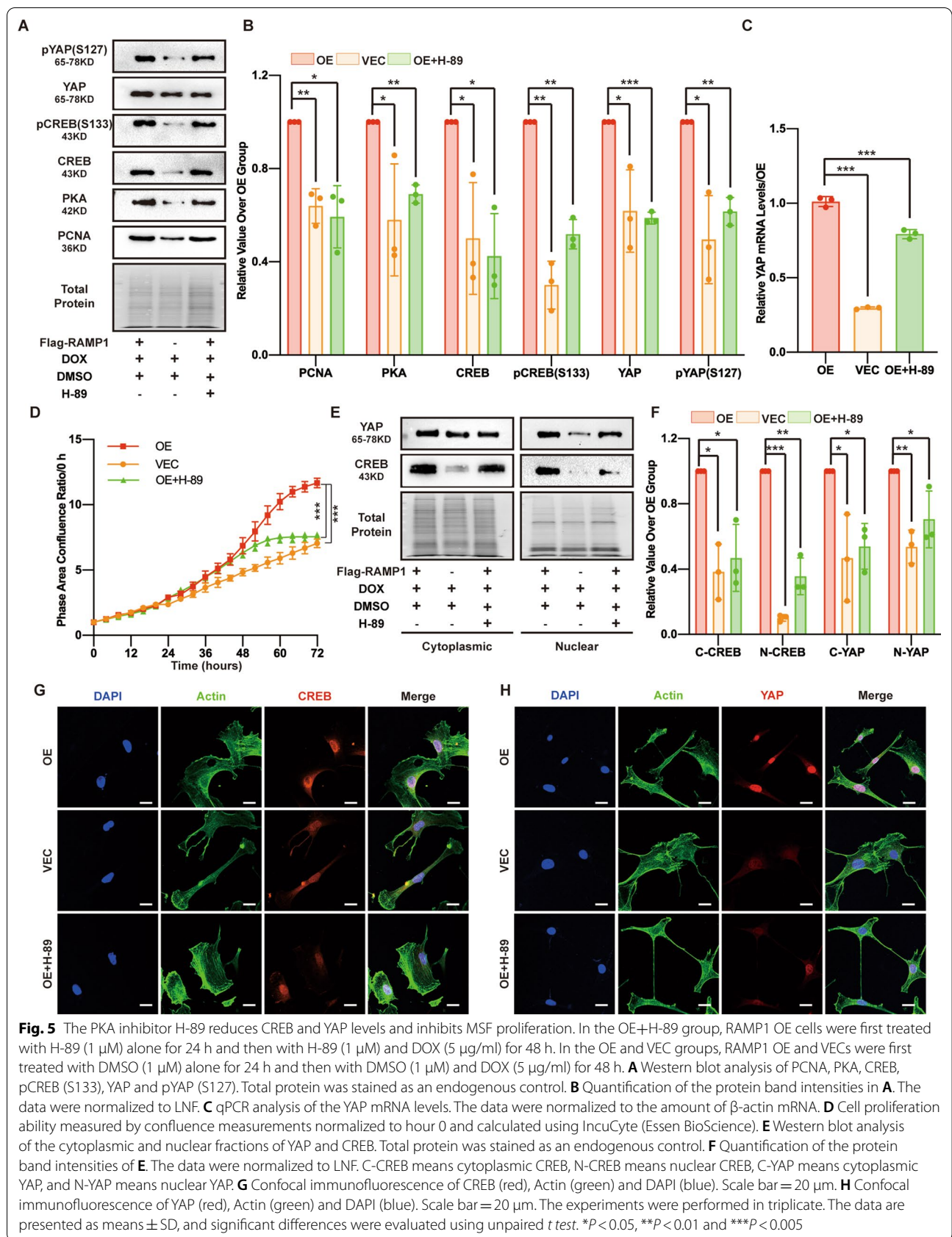


**Fig. 4** (See legend on previous page.)

**The PKA agonist BUC increases CREB and YAP expression and MSF proliferation**

We used the PKA agonist BUC (0.01 μM) to identify the role of PKA in YAP activity regulation and proliferation rate of RAMP1-overexpressing cells. Consistently, BUC elevated the MSF proliferation rate, as evaluated by the

cell confluence area ratio measured by the S3 instrument and by the expression of the proliferation marker PCNA as measured by Western blotting (Fig. 6A, B, D). To determine downstream PKA, CREB and YAP protein levels and YAP transcription levels, BUC treatment was administered, revealing a positive effect (Fig. 6A–C).



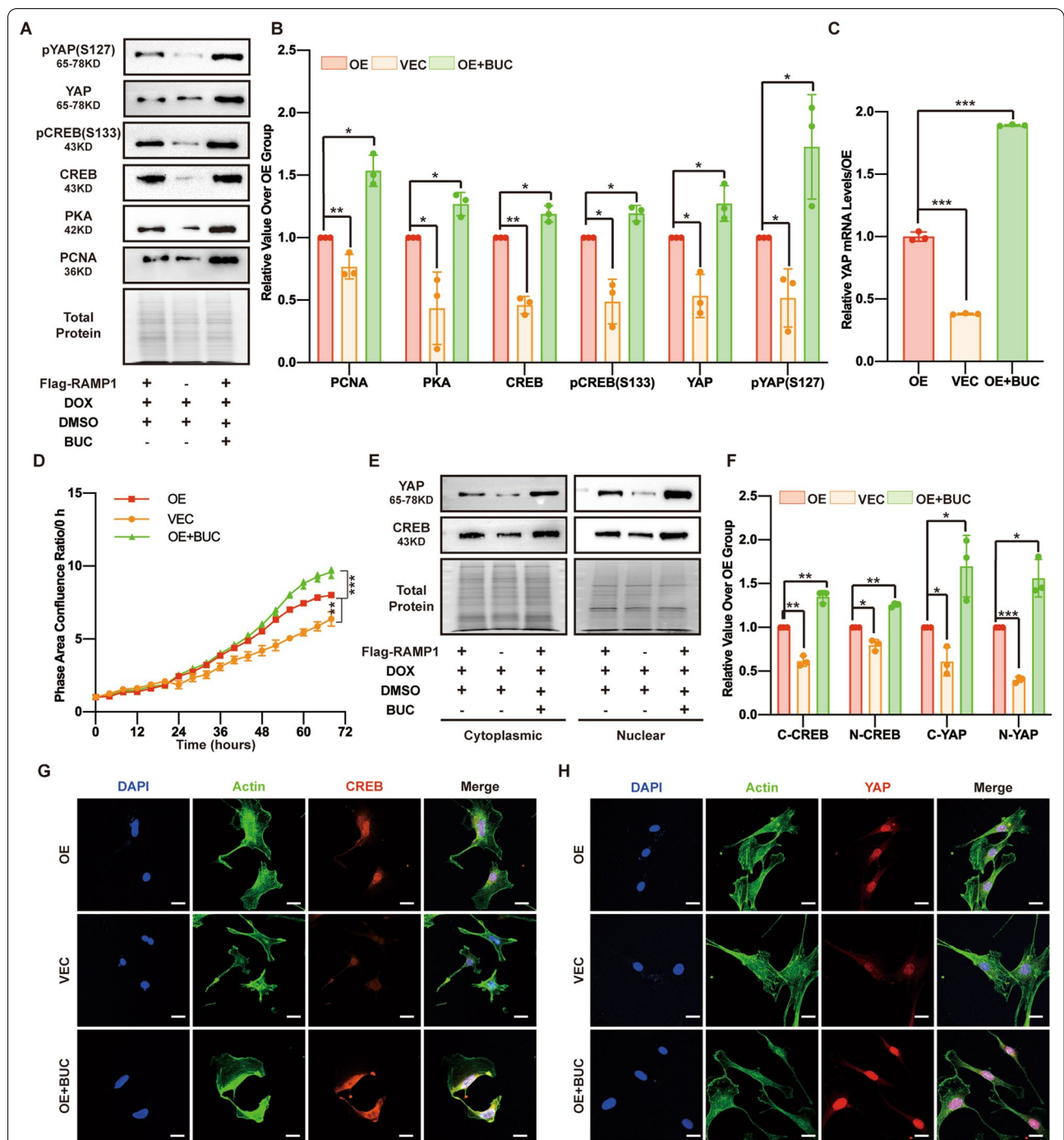


**Fig. 6** The PKA agonist BUC increases CREB and YAP expression and MSF proliferation. In the OE+BUC group, RAMP1 OE cells were first treated with DOX (5 µg/ml) for 48 h and then with BUC (0.01 µM) and DOX (5 µg/ml) for 24 h. In the OE and VEC groups, RAMP1 OE and VECs were first treated with DOX (5 µg/ml) for 48 h and then DMSO (0.01 µM) and DOX (5 µg/ml) for 24 h. **A** Western blot analysis of PCNA, PKA, CREB, pCREB (S133), YAP and pYAP (S127). Total protein was stained as an endogenous control. **B** Quantification of the protein band intensities in **A**. The data were normalized to LNF. **C** qPCR analysis of the YAP mRNA levels. The data were normalized to the amount of β-actin mRNA. **D** Cell proliferation ability measured by confluence measurements normalized to hour 0 and calculated using IncuCyte (Essen BioScience). **E** Western blot analysis of the cytoplasmic and nuclear fractions of YAP and CREB. Total protein was stained as an endogenous control. **F** Quantification of the protein band intensities of **E**. The data were normalized to LNF. C-CREB means cytoplasmic CREB, N-CREB means nuclear CREB, C-YAP means cytoplasmic YAP, and N-YAP means nuclear YAP. **G** Confocal immunofluorescence of CREB (red), Actin (green) and DAPI (blue). Scale bar = 20 µm. **H** Confocal immunofluorescence of YAP (red), Actin (green) and DAPI (blue). Scale bar = 20 µm. The experiments were performed in triplicate. The data are presented as means ± SD, and significant differences were evaluated using unpaired *t* test. \**P* < 0.05, \*\**P* < 0.01 and \*\*\**P* < 0.005

Interestingly, BUC increased the level of the CREB active form, pCREB (S133), and the YAP inactive form, pYAP (S127) (Fig. 6A, B). Next, we explored the effect of BUC on CREB and YAP cell localization, revealing that BUC caused increased cytoplasmic and nuclear localization of YAP and CREB (Fig. 6E–H). We also observed that the wound closure percentage of the BUC (100 nmol)-treated side was higher at each corresponding observation time point than that of the DMSO-treated side (Additional file 2: Fig. S1G and S1H), indicating that stimulation of PKA by BUC may promote the wound healing rate. Taken together, these results indicate that RAMP1-Gai3 modulates MSF proliferation by regulating PKA function, but the pathway components remain to be identified.

### The RAMP1-Gai3-PKA axis regulates YAP mediated by CREB

Because CREB is the most common downstream factor of PKA and the abovementioned results showed that CREB is regulated by the RAMP1-Gai3-PKA axis, we asked whether CREB can regulate YAP levels and whether this regulation is accomplished at the transcriptional level. To identify the regulatory effect of CREB on YAP, we first administered KG-501 (10  $\mu$ M), a CREB activity inhibitor, to RAMP1-OE cells and observed a decreased proliferation rate by the S3 assay and Western blotting and IF staining for PCNA (Fig. 7A–E). As speculated, KG-501 diminished YAP and pYAP (S127) levels in the OE+KG-501 group. Interestingly, although KG-501 was first found to function by inhibiting the binding of CREB [38], we also observed that the CREB and pCREB (S133) levels were reduced by KG-501 (Fig. 7C, D) and the level of cytoplasmic CREB and that of nuclear CREB was reduced (Fig. 7G–I). Additionally, KG-501 treatment led to a decrease in both cytoplasmic and nuclear YAP levels and reduced YAP mRNA transcription (Fig. 7F, G, H, J). Next, we evaluated CREB transcriptional activity in relation to YAP levels. The JASPAR database was used to analyse CBSs in *YAP* promoter sequences (Additional

file 3: Fig. S2A). The three candidate sites with the highest predicted score were –818 to 825 bp, –2664 to 2671 bp and –1204 to 1211 bp in *YAP* promoter (Additional file 1: Table S4). To determine whether CREB binds at these sites to target *YAP* promoter, we performed a CUT&RUN assay, and the qPCR and agarose gel electrophoresis results confirmed that CREB can directly bind to the *YAP* promoter at these three sites (Additional file 3: Fig. S2B; Fig. 7K). Next, to determine whether these candidate sites are cAMP responsive elements (CREs), we performed a luciferase promoter activity assay, revealing that CREB could transactivate the wild-type reporter construct but failed to transactivate the mutation reporter with the deletion of the above three predicted binding sites, indicating that CREB can act on at least one of the three sites on the *YAP* promoter region (Fig. 7L). Further experiments are needed to identify which sites are the most functional. We also performed an in vivo experiment by administering KG-501 (100 nmol) on skin wounds on the right side and found that KG-501 significantly slowed the wound closure rate (Additional file 2: Fig. S1I and S1J) compared with the control group on the other side, indicating that the CREB inhibitor KG-501 could slow wound healing, particularly at the early stage. Together, these results indicate that the RAMP1-Gai3-PKA axis can regulate YAP levels and MSF proliferation mediated by CREB and that CREB can bind to the *YAP* promoter and promote YAP transcription.

### Discussion

Abnormal skin innervation can lead to abnormal skin wound healing, which includes an excessive wound healing process, such as scarring, or inadequate wound healing, such as the formation of chronic nonhealing ulcers and ischaemic chronic wounds [6, 9, 14, 39, 40]. CGRP-positive nerve endings are among the most widely distributed peptidergic nerve fibres and play a crucial role in normal wound healing [8, 40]. However, CGRP causes many side effects directly in wounds [41, 42]. Recently,

(See figure on next page.)

**Fig. 7** The RAMP1-Gai3-PKA axis regulates YAP mediated by CREB. In the OE+KG-501 group, RAMP1 OE cells were first treated with KG-501 (10  $\mu$ M) for 12 h and then with KG-501 (10  $\mu$ M) and DOX (5  $\mu$ g/ml) for 48 h. In the OE and VEC groups, RAMP1 OE and VECs were first treated with DMSO (10  $\mu$ M) for 12 h and then with DMSO (10  $\mu$ M) and DOX (5  $\mu$ g/ml) for 48 h. **A** Confocal immunofluorescence of PCNA (red), Actin (green) and DAPI (blue). Scale bar = 20  $\mu$ m. **B** Dot plots show quantification of the frequency of PCNA-positive cells in each field of view. **C** Western blot analysis of PCNA, CREB, pCREB (S133), YAP and pYAP (S127). Total protein was stained as an endogenous control. **D** Quantification of the protein band intensities in **C**. The data were normalized to LNF. **E** Cell proliferation ability measured by confluence measurements normalized to hour 0 and calculated using IncuCyte (Essen BioScience). **F** qPCR analysis of the *YAP* mRNA levels. The data were normalized to the amount of  $\beta$ -actin mRNA. **G** Western blot analysis of the cytoplasmic and nuclear fractions of YAP and CREB. Total protein was stained as an endogenous control. **H** Quantification of the protein band intensities of **G**. The data were normalized to LNF. C-CREB means cytoplasmic CREB, N-CREB means nuclear CREB, C-YAP means cytoplasmic YAP, and N-YAP means nuclear YAP. **I** Confocal immunofluorescence of CREB (red), Actin (green) and DAPI (blue). Scale bar = 20  $\mu$ m. **J** Confocal immunofluorescence of YAP (red), Actin (green) and DAPI (blue). Scale bar = 20  $\mu$ m. **K** DNA agarose gel electrophoresis of *YAP* promoter DNA quantification using the CUT&RUN assay and qPCR with different primers. **L** Dual-luciferase reporter assay of the CBS wild-type (WT) *YAP* promoter and mutated (Mut) *YAP* promoter. The experiments were performed in triplicate. The data were presented as means  $\pm$  SD, and significant differences were evaluated using unpaired *t* test. \**P* < 0.05, \*\**P* < 0.01, \*\*\**P* < 0.005 and ns, not significant

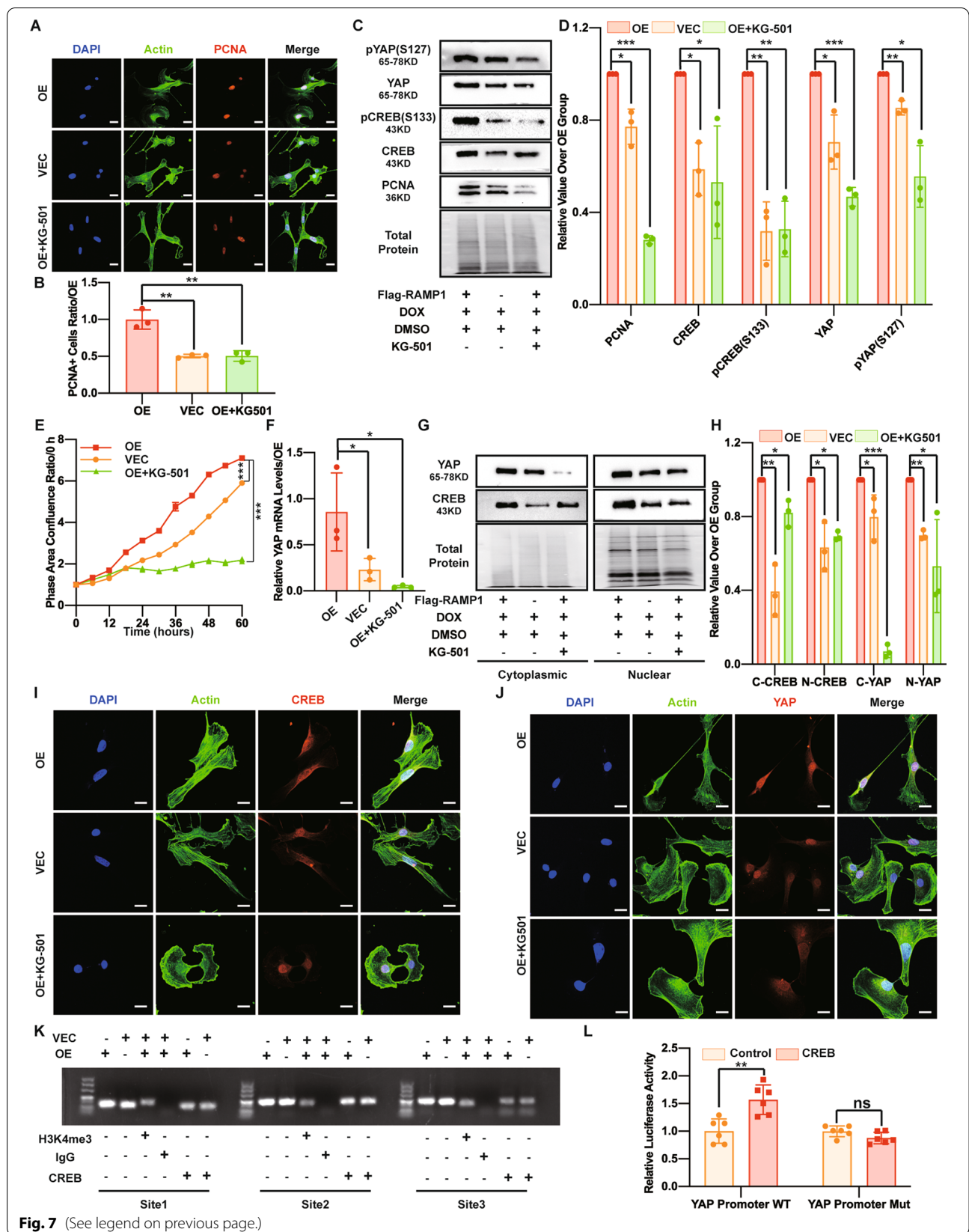


**Fig. 7** (See legend on previous page.)

RAMP1 was reported to promote wound healing by increasing angiogenesis and lymphangiogenesis [20], suggesting that CGRP function can be modulated by manipulating RAMP1. However, few studies on RAMP1 and skin cells have been performed; therefore, it is necessary to explore the function of RAMP1 in skin cells and verify the downstream regulatory mechanism.

In the present study, we first identified that RAMP1 levels change during wound healing, suggesting that RAMP1 functions during the wound healing process. Next, we successfully constructed a RAMP1-overexpressing MSF cell line in vitro and found that it can promote MSF proliferation. By performing mechanistic studies, we found that the effect of RAMP1 OE on MSF proliferation was mainly mediated by the G $\alpha$ i3-PKA-CREB-YAP axis, leading to upregulated transcription of YAP, increased nuclear YAP levels and an elevated MSF proliferation rate. In vivo experiments confirmed the role of G $\alpha$ i3-PKA-CREB-YAP axis molecules in wound healing.

RAMP1 is a member of the RAMP family, which includes two other identified members, RAMP2 and RAMP3 [19, 43]. RAMP1 was first identified during an effort to understand CGRP signalling, and it can modify CLR downstream signalling, traffic CLR to the cell surface, and affect CLR internalization [43]. However, the distribution of RAMP1 is wider than that of CLR [43, 44], and Debbie et al. reported that the cortex and hippocampus expressed RAMP1 but not CLR [45], indicating that RAMP1 has functions other than those related to CLR. Previous studies of RAMP1 focused primarily on its effect on exogenous or endogenous CGRP function, and the function of RAMP1 alone on fibroblasts has not been previously explored. In this study, we explored, without using exogenous CGRP, whether RAMP1 alone can affect MSF function. We observed that RAMP1 OE alone can promote MSF proliferation, indicating, for the first time, that RAMP1 alone can exert an effect, but exploration into its downstream regulatory mechanism is necessary.

RAMPs have been reported to promote G protein uncoupling [46] and alter the association of GPCR coupling to G proteins, in addition to G $\alpha$ s, G $\alpha$ q, and G $\alpha$ i [47]. We found that with RAMP1 OE, the G $\alpha$ i3 level was increased, and the downstream PKA and CREB levels were elevated. G $\alpha$ i3 is one of the three inhibitory subunits of G proteins that can inhibit AC activity, leading to decreased cAMP production and PKA activity [48]. However, G $\alpha$ i3 has also been shown to stimulate AC2 and AC4 to increase cAMP levels and PKA activity [29]. The current study indicated that RAMP1 OE can upregulate G $\alpha$ i3 to promote PKA activity, but whether it was performed by stimulating AC2 or AC4 remains to be verified in our subsequent study.

PKA has been reported to phosphorylate LATS1/2 and thus phosphorylate YAP, which mostly occurs at S127 and leads to Hippo pathway activation [30, 31, 49], and we observed elevated pYAP (S127), consistent with a previously reported study. Although the elevated Ser127 phosphorylation of YAP has been linked to the functional inactivation of YAP through cytoplasmic retention and degradation [50, 51] and we found that the cytoplasmic YAP level was higher in the RAMP1 OE group than in the control group, we observed that the nuclear YAP level was also higher in the OE group, indicating that the total YAP protein level was elevated. In other words, the transcription and synthesis of YAP were both increased; hence, although YAP was retained in the cytoplasm, YAP translocation into the nucleus remained high. CREB has been reported to be a transcription factor of YAP in hepatoma cells [32, 52]. In our study, using the CUT&RUN assay and dual-luciferase reporter assays, CREB could bind to sites in the YAP promoter and functioned as a transcription factor. We clarify that CREB is a YAP transcription factor in MSFs, but the specific site must be verified using dual luciferase reporter assays at different mutation sites.

CREB, a 43 kDa amino acid, is the classic downstream factor of PKA. As a transcription factor, it functions by binding to the CRE with coactivators, such as CREB-binding protein (CBP), to activate the downstream transcriptional signal [53, 54]. Phosphorylation of amino acid residues is the regulatory mechanism of CREB, and different phosphorylation patterns serve different functions, among which the Ser133 residue frequently occurs and induces transcription, while Ser111 occurs less frequently and inhibits transcription [54, 55]. In our study, elevated CREB and pCREB (S133) were observed in total protein extracts and subcellular protein extracts, indicating that activated CREB was a downstream factor of RAMP1 OE. KG-501 was first identified by Best et al. [38] as a CREB-CBP inhibitor, and Steven A et al. [56] reported that KG-501 could decrease Her-2/neu-overexpressing cell migration without influencing CREB expression and phosphorylation. In our study, KG-501 treatment did not influence the CREB transcription level (data not shown); however, we also observed decreased CREB protein levels not only in total protein extracts but also in cytoplasmic and nuclear proteins, and the pCREB (S133) level was also reduced, indicating that CREB degradation might be increased by KG-501 treatment. Wang et al. [32] reported that YAP may help stabilize CREB by inhibiting mitogen-activated protein kinase 14 (MAPK14/p38) and beta-transducin repeat containing E3 ubiquitin protein ligase (BTRC). Therefore, the decreased CREB level and pCREB (S133) in the OE+KG-501 group may be explained by the

decreased YAP level induced by KG-501 treatment. However, the exact mechanism by which KG-501 treatment leads to decreased CREB levels in MSF cell lines requires further experimental exploration.

However, some limitations existed concerning the *in vivo* experiments. We only identified the RAMP1 expression of wound tissue protein during wound healing by Western blot analysis and IHC staining analysis, but not other molecules in the Gai3-PKA-CREB-YAP axis signalling pathway. We can theoretically conclude that the axis was also the signalling pathway by which RAMP1 regulates wound healing because these pathway interventions significantly affected the early phase of wound healing and the expression level of RAMP1 gradually increased during the early phase of the wound healing process, which is also the proliferative phase where fibroblasts play a crucial role [3, 5]. However, we can only logically obtain the result that the intervention could change the wound healing process and that the corresponding molecule was important for wound healing. A complete understanding of the detailed confirmation of the mechanism awaits further studies that may require RAMP1 transgenic mice; however, animals are currently unavailable.

## Conclusions

In summary, our study identified, for the first time, that total RAMP1 levels change during skin wound healing and that RAMP1 OE alone can promote MSF proliferation by activating Gai3 and downstream PKA and CREB, leading to *YAP* transcription and elevated nuclear YAP levels. The results of this study expand our knowledge of RAMP1 function and serve as the basis to exploit RAMP1 as a target in the treatment of skin wounds.

## Abbreviations

CGRP: Calcitonin gene-related peptide; RAMP1: Receptor activity-modifying protein 1; MSF: Mouse skin fibroblast; DOX: Doxycycline; qPCR: Quantitative real-time polymerase chain reaction; IF: Immunofluorescence; YAP: Yes-associated protein; G protein: Guanine nucleotide-binding protein; Gai3: Inhibitory guanine nucleotide-binding protein (G protein)  $\alpha$  subunit 3; PKA: Protein kinase A; cAMP: Cyclic adenosine monophosphate; CREB: Cyclic adenosine monophosphate (cAMP) response element-binding protein; CLR: Calcitonin receptor-like receptor; RCP: Receptor component protein; GPCR: G protein-coupled receptor; Gas: Stimulatory G $\alpha$  subunit; AC: Adenylyl cyclase; Gai: Inhibitory G $\alpha$  subunit; DMEM: Dulbecco's modified Eagle's medium; FBS: Foetal bovine serum; BUC: Bucladesine sodium; VP: Verteporfin; DMSO: Dimethyl sulfoxide; siRNAs: Small interfering RNAs; H&E: Hematoxylin–eosin; IHC: Immunohistochemical; DAB: Diaminobenzidine; IOD: Integrated optical density; PBS: Phosphate-buffered saline; HRP: Horseradish peroxidase; CUT&RUN: Cleavage under targets & release using nuclease; mAb: Monoclonal antibody; H3K4me3: Trimethylated histone H3 (Lys4); CBS: CREB-binding site; SD: Standard deviation; VEC: Vector control; OE: Overexpression; CRE: CAMP responsive element; CBP: CREB-binding protein; MAPK14: Mitogen-activated protein kinase 14; BTRC: Beta-transducin repeat containing E3 ubiquitin protein ligase; LNF: Lane normalization factor; WT: Wild-type; Mut: Mutated.

## Supplementary Information

The online version contains supplementary material available at <https://doi.org/10.1186/s12964-022-00852-0>.

**Additional file 1: Table S1.** Primer sequences used in lentivirus over-expression. **Table S2.** siRNA target sequences used for gene expression interference. **Table S3.** Primer sequences used for PCR amplification. **Table S4.** Predicted CBSs on the YAP promoter.

**Additional file 2: Fig. S1.** (A) Typical appearance of wounds on the DMSO (10  $\mu$ l)-treated control side (Ctrl) and VP (100 nmol)-treated side (VP) at 0 hours (days 0), 24 hours (days 1), days 3, days 5 and days 7 post-injury. (B) Time course of the wound closure rates of the DMSO- and VP-treated sides. (C) Typical appearance of wounds on the siNC (5 nmol)-treated control side (siNC) and siGai3-2 (5 nmol)-treated side (siGai3-2) at 0 hours (days 0), 24 hours (days 1), days 3, days 5 and days 7 post-injury. (D) Time course of the wound closure rates of the siNC- and siGai3-2-treated sides. (E) Typical appearance of wounds on the DMSO (10  $\mu$ l)-treated control side (Ctrl) and H-89 (100 nmol)-treated side (H-89) at 0 hours (days 0), 24 hours (days 1), days 3, days 5 and days 7 post-injury. (F) Time course of the wound closure rates of the DMSO- and H-89-treated sides. (G) Typical appearance of wounds on the DMSO (10  $\mu$ l)-treated control side (Ctrl) and BUC (100 nmol)-treated side (BUC) at 0 hours (days 0), 24 hours (days 1), days 3, days 5 and days 7 post-injury. (H) Time course of the wound closure rates of the DMSO- and BUC-treated sides. (I) Typical appearance of wounds on the DMSO (10  $\mu$ l)-treated control side (Ctrl) and KG-501 (100 nmol)-treated side (KG-501) at 0 hours (days 0), 24 hours (days 1), days 3, days 5 and days 7 post-injury. (J) Time course of the wound closure rates of the DMSO- and KG-501-treated sides. The data are presented as means  $\pm$  SD, and significant differences were evaluated using unpaired *t* test. \**P* < 0.05, \*\**P* < 0.01, \*\*\**P* < 0.005

**Additional file 3: Fig. S2.** (A) CBSs in *YAP* promoter sequences analysed using the JASPAR database. (B) CUT&RUN assay and qPCR of CBSs on the *YAP* promoter. The experiments were performed in triplicate. The data are presented as means  $\pm$  SD, and significant differences were evaluated using unpaired *t* test. \**P* < 0.05, \*\**P* < 0.01 and \*\*\**P* < 0.005.

## Acknowledgements

Not applicable.

## Author contributions

SY, RS and YW designed the work. SY and RS performed the most experiments, analysed the data. RS wrote the manuscript and SY substantively revised it. JM, ZW, GC and GZ performed part of the experiments. YW performed funding acquisition and manuscript review and edit. CL provided expert technical assistance and supervised the project. JL, HZ, RS and AC performed project validation. All authors read and approved the final manuscript.

## Funding

This study was supported by the National Natural Science Foundation of China (81972947), Natural Science Foundation of Shandong Province of China (Major Basic Research Program) (ZR2019ZD38), Academic Promotion Program of Shandong First Medical University (2019LJ005) and Jinan Clinical Research Center for Tissue Engineering Skin Regeneration and Wound Repair.

## Availability of data and materials

All data generated or analysed during this study are included in this published article and its Additional information files.

## Declarations

### Ethics approval and consent to participate

All the experiments were approved by the ethics committee of The First Affiliated Hospital of Shandong First Medical University & Shandong Provincial Qianfoshan Hospital (Approval Number: SYDWLS[2021]002).

**Consent for publication**

Not applicable.

**Competing interests**

The authors declare that they have no competing interests.

**Author details**

<sup>1</sup>Department of Plastic Surgery, Shandong Provincial Qianfoshan Hospital, Cheeloo College of Medicine, Shandong University, Jinan 250012, Shandong, People's Republic of China. <sup>2</sup>Jinan Clinical Research Center for Tissue Engineering Skin Regeneration and Wound Repair, The First Affiliated Hospital of Shandong First Medical University & Shandong Provincial Qianfoshan Hospital, Jinan 250014, Shandong, People's Republic of China. <sup>3</sup>Department of Plastic Surgery, The First Affiliated Hospital of Shandong First Medical University & Shandong Provincial Qianfoshan Hospital, Jinan 250014, Shandong, People's Republic of China.

Received: 9 November 2021 Accepted: 1 March 2022

Published online: 12 April 2022

**References**

- Rognoni E, Watt FM. Skin cell heterogeneity in development, wound healing, and cancer. *Trends Cell Biol.* 2018;28(9):709–22.
- Dekoninck S, Blanpain C. Stem cell dynamics, migration and plasticity during wound healing. *Nat Cell Biol.* 2019;21(1):18–24.
- Rodrigues M, Kosaric N, Bonham CA, Gurtner GC. Wound healing: a cellular perspective. *Physiol Rev.* 2019;99(1):665–706.
- Gurtner GC, Werner S, Barrandon Y, Longaker MT. Wound repair and regeneration. *Nature.* 2008;453(7193):314–21.
- Tracy LE, Minasian RA, Caterson EJ. Extracellular Matrix and dermal fibroblast function in the healing wound. *Adv Wound Care (New Rochelle).* 2016;5(3):119–36.
- Chéret J, Lebonvallet N, Carré JL, Misery L, Le Gall-Ianotto C. Role of neuropeptides, neurotrophins, and neurohormones in skin wound healing. *Wound Repair Regen.* 2013;21(6):772–88.
- Toda M, Suzuki T, Hosono K, Kurihara Y, Kurihara H, Hayashi I, et al. Roles of calcitonin gene-related peptide in facilitation of wound healing and angiogenesis. *Biomed Pharmacother.* 2008;62(6):352–9.
- Chéret J, Lebonvallet N, Buhé V, Carre JL, Misery L, Le Gall-Ianotto C. Influence of sensory neuropeptides on human cutaneous wound healing process. *J Dermatol Sci.* 2014;74(3):193–203.
- Laverdet B, Danigo A, Girard D, Magy L, Demiot C, Desmoulière A. Skin innervation: important roles during normal and pathological cutaneous repair. *Histol Histopathol.* 2015;30(8):875–92. <https://doi.org/10.14670/HH-11-610>.
- Ashrafi M, Baguneid M, Bayat A. The role of neuromediators and innervation in cutaneous wound healing. *Acta Derm Venereol.* 2016;96(5):587–94.
- Roggenkamp D, Köpnick S, Stäb F, Wenck H, Schmelz M, Neufang G. Epidermal nerve fibers modulate keratinocyte growth via neuropeptide signaling in an innervated skin model. *J Invest Dermatol.* 2013;133(6):1620–8.
- Alapure BV, Lu Y, Peng H, Hong S. Surgical denervation of specific cutaneous nerves impedes excisional wound healing of small animal ear pinnae. *Mol Neurobiol.* 2018;55(2):1236–43.
- Kant V, Kumar D, Kumar D, Prasad R, Gopal A, Pathak NN, et al. Topical application of substance P promotes wound healing in streptozotocin-induced diabetic rats. *Cytokine.* 2015;73(1):144–55.
- Ishikawa S, Takeda A, Akimoto M, Kounoike N, Uchinuma E, Uezono Y. Effects of neuropeptides and their local administration to cutaneous wounds in sensory-impaired areas. *J Plast Surg Hand Surg.* 2014;48(2):143–7.
- Lebonvallet N, Boulais N, Gall CL, Pereira U, Gauché D, Gobin E, et al. Effects of the re-innervation of organotypic skin explants on the epidermis. *Exp Dermatol.* 2012;21(2):156–8.
- Russell FA, King R, Smillie SJ, Kodji X, Brain SD. Calcitonin gene-related peptide: physiology and pathophysiology. *Physiol Rev.* 2014;94(4):1099–142.
- Rosenfeld MG, Mermod JJ, Amara SG, Swanson LW, Sawchenko PE, Rivier J, et al. Production of a novel neuropeptide encoded by the calcitonin gene via tissue-specific RNA processing. *Nature.* 1983;304(5922):129–35.
- Evans BN, Rosenblatt MI, Mnayer LO, Oliver KR, Dickerson IM. CGRP-RCP, a novel protein required for signal transduction at calcitonin gene-related peptide and adrenomedullin receptors. *J Biol Chem.* 2000;275(40):31438–43.
- Serafin DS, Harris NR, Nielsen NR, Mackie DI, Caron KM. Dawn of a new RAMPPage. *Trends Pharmacol Sci.* 2020;41(4):249–65.
- Kurashige C, Hosono K, Matsuda H, Tsujikawa K, Okamoto H, Majima M. Roles of receptor activity-modifying protein 1 in angiogenesis and lymphangiogenesis during skin wound healing in mice. *FASEB J Off Publ Feder Am Soc Exp Biol.* 2014;28(3):1237–47. <https://doi.org/10.1096/fj.13-238998>.
- Mishima T, Ito Y, Nishizawa N, Amano H, Tsujikawa K, Miyaji K, et al. RAMP1 signaling improves lymphedema and promotes lymphangiogenesis in mice. *J Surg Res.* 2017;219:50–60.
- Rognoni E, Walko G. The roles of YAP/TAZ and the hippo pathway in healthy and diseased skin. *Cells.* 2019;8(5):411.
- Walko G, Woodhouse S, Pisco AO, Rognoni E, Liakath-Ali K, Lichtenberger BM, et al. A genome-wide screen identifies YAP/WBP2 interplay conferring growth advantage on human epidermal stem cells. *Nat Commun.* 2017;8:14744.
- Yu FX, Zhao B, Guan KL. Hippo pathway in organ size control, tissue homeostasis, and cancer. *Cell.* 2015;163(4):811–28.
- Luo J, Yu FX. GPCR-Hippo signaling in cancer. *Cells.* 2019;8(5):426.
- Walker CS, Conner AC, Poyner DR, Hay DL. Regulation of signal transduction by calcitonin gene-related peptide receptors. *Trends Pharmacol Sci.* 2010;31(10):476–83.
- Laschinger M, Wang Y, Holzmann G, Wang B, Stöb C, Lu M, et al. The CGRP receptor component RAMP1 links sensory innervation with YAP activity in the regenerating liver. *FASEB J.* 2020;34(6):8125–38.
- Wang W, Qiao Y, Li Z. New insights into modes of GPCR activation. *Trends Pharmacol Sci.* 2018;39(4):367–86.
- Baker LP, Nielsen MD, Impey S, Hacker BM, Poser SW, Chan MY, et al. Regulation and immunohistochemical localization of betagamma-stimulated adenylyl cyclases in mouse hippocampus. *J Neurosci.* 1999;19(1):180–92.
- Yu FX, Zhang Y, Park HW, Jewell JL, Chen Q, Deng Y, et al. Protein kinase A activates the Hippo pathway to modulate cell proliferation and differentiation. *Genes Dev.* 2013;27(11):1223–32.
- Zhang L, Noguchi YT, Nakayama H, Kaji T, Tsujikawa K, Ikemoto-Uezumi M, et al. The CalcR-PKA-Yap1 axis is critical for maintaining quiescence in muscle stem cells. *Cell Rep.* 2019;29(8):2154–63.e5.
- Wang J, Ma L, Weng W, Qiao Y, Zhang Y, He J, et al. Mutual interaction between YAP and CREB promotes tumorigenesis in liver cancer. *Hepatology.* 2013;58(3):1011–20.
- Zhang M, Zhang R, Li X, Cao Y, Huang K, Ding J, et al. CD271 promotes STZ-induced diabetic wound healing and regulates epidermal stem cell survival in the presence of the pTrkA receptor. *Cell Tissue Res.* 2020;379(1):181–93.
- Zhang M, Zhang Y, Ding J, Li X, Zang C, Yin S, et al. The role of TrkA in the promoting wounding-healing effect of CD271 on epidermal stem cells. *Arch Dermatol Res.* 2018;310(9):737–50.
- Zhang M, Cao Y, Li X, Hu L, Taieb SK, Zhu X, et al. Cd271 mediates proliferation and differentiation of epidermal stem cells to support cutaneous burn wound healing. *Cell Tissue Res.* 2018;371(2):273–82.
- Liu Z, Cao Y, Liu G, Yin S, Ma J, Liu J, et al. p75 neurotrophin receptor regulates NGF-induced myofibroblast differentiation and collagen synthesis through MRTF-A. *Exp Cell Res.* 2019;383(1):111504.
- Wang C, Zhu X, Feng W, Yu Y, Jeong K, Guo W, et al. Verteporfin inhibits YAP function through up-regulating 14–3–3 $\sigma$  sequestering YAP in the cytoplasm. *Am J Cancer Res.* 2016;6(1):27–37.
- Best JL, Amezcua CA, Mayr B, Flechner L, Murawsky CM, Emerson B, et al. Identification of small-molecule antagonists that inhibit an activator: coactivator interaction. *Proc Natl Acad Sci U S A.* 2004;101(51):17622–7.
- Goldberg SR, Diegelmann RF. Wound healing primer. *Surg Clin North Am.* 2010;90(6):1133–46.
- Martínez-Greene JA, Martínez-Martínez E. Influence of sensory innervation on epithelial renewal and wound healing. In: Shiffman M, Low M, editors. *Vascular surgery, neurosurgery, lower extremity ulcers,*

antimicrobials, wound assessment, care, measurement and repair. Recent clinical techniques, results, and research in wounds, vol. 5. Cham: Springer; 2018. [https://doi.org/10.1007/15695\\_2018\\_130](https://doi.org/10.1007/15695_2018_130).

41. Choi JE, Di Nardo A. Skin neurogenic inflammation. *Semin Immunopathol.* 2018;40(3):249–59.
42. Sousa-Valente J, Brain SD. A historical perspective on the role of sensory nerves in neurogenic inflammation. *Semin Immunopathol.* 2018;40(3):229–36.
43. Klein KR, Matson BC, Caron KM. The expanding repertoire of receptor activity modifying protein (RAMP) function. *Crit Rev Biochem Mol Biol.* 2016;51(1):65–71.
44. Udawela M, Hay DL, Sexton PM. The receptor activity modifying protein family of G protein coupled receptor accessory proteins. *Semin Cell Dev Biol.* 2004;15(3):299–308.
45. Hay DL, Poyner DR, Sexton PM. GPCR modulation by RAMPs. *Pharmacol Ther.* 2006;109(1–2):173–97.
46. Weston C, Lu J, Li N, Barkan K, Richards GO, Roberts DJ, et al. Modulation of glucagon receptor pharmacology by receptor activity-modifying protein-2 (RAMP2). *J Biol Chem.* 2015;290(38):23009–22.
47. Wootten D, Lindmark H, Kadmiel M, Willcockson H, Caron KM, Barwell J, et al. Receptor activity modifying proteins (RAMPs) interact with the VPAC2 receptor and CRF1 receptors and modulate their function. *Br J Pharmacol.* 2013;168(4):822–34.
48. Alessi DR, James SR, Downes CP, Holmes AB, Gaffney PR, Reese CB, et al. Characterization of a 3-phosphoinositide-dependent protein kinase which phosphorylates and activates protein kinase Balpha. *Curr Biol.* 1997;7(4):261–9.
49. Kim M, Kim M, Lee S, Kuninaka S, Saya H, Lee H, et al. cAMP/PKA signalling reinforces the LATS-YAP pathway to fully suppress YAP in response to actin cytoskeletal changes. *Embo j.* 2013;32(11):1543–55.
50. Zhao B, Li L, Tumaneng K, Wang CY, Guan KL. A coordinated phosphorylation by Lats and CK1 regulates YAP stability through SCF(beta-TRCP). *Genes Dev.* 2010;24(1):72–85.
51. Zhao B, Wei X, Li W, Udan RS, Yang Q, Kim J, et al. Inactivation of YAP oncoprotein by the Hippo pathway is involved in cell contact inhibition and tissue growth control. *Genes Dev.* 2007;21(21):2747–61.
52. Zhang T, Zhang J, You X, Liu Q, Du Y, Gao Y, et al. Hepatitis B virus X protein modulates oncogene Yes-associated protein by CREB to promote growth of hepatoma cells. *Hepatology.* 2012;56(6):2051–9.
53. Montminy MR, Bilezikjian LM. Binding of a nuclear protein to the cyclic-AMP response element of the somatostatin gene. *Nature.* 1987;328(6126):175–8.
54. Steven A, Friedrich M, Jank P, Heimer N, Budczies J, Denkert C, et al. What turns CREB on? And off? And why does it matter? *Cell Mol Life Sci.* 2020;77(20):4049–67.
55. Johannessen M, Delghandi MP, Moens U. What turns CREB on? *Cell Signal.* 2004;16(11):1211–27.
56. Steven A, Leisz S, Massa C, Iezzi M, Lattanzio R, Lamolinara A, et al. HER-2/neu mediates oncogenic transformation via altered CREB expression and function. *Mol Cancer Res.* 2013;11(11):1462–77.

## Publisher's Note

Springer Nature remains neutral with regard to jurisdictional claims in published maps and institutional affiliations.

Ready to submit your research? Choose BMC and benefit from:

- fast, convenient online submission
- thorough peer review by experienced researchers in your field
- rapid publication on acceptance
- support for research data, including large and complex data types
- gold Open Access which fosters wider collaboration and increased citations
- maximum visibility for your research: over 100M website views per year

At BMC, research is always in progress.

Learn more [biomedcentral.com/submissions](https://biomedcentral.com/submissions)

